Research Article

Ahlam Zekaik, Hadj Benhebal*, and Bedhiaf Benrabah

Synthesis and characterization of Cu doped chromium oxide (Cr_2O_3) thin films

https://doi.org/10.1515/htmp-2019-0037
Received Jun 08, 2018; accepted Feb 12, 2019

Abstract: Cu-doped Cr_2O_3 thin films were deposited onto glass substrate by the sol–gel dip-coating (SGDC) process using dopant values of 0, 3, 6, 9 and 12%. The Chromium (III) Nitrate Nonahydrate [$Cr(NO_3)_3{\cdot}9H_2O$] was used as a Cr source, whilst for the dopant, the corresponding nitrate ($Cu(NO_3)_2$) was used. The crystal structure, as well as the optical and electrical properties were examined. XRD data showed that the films with a high degree of crystallinity were rhombohedral Cr_2O_3 phase. The crystallite size reduces with increase in Cu doping proportion. The AFM results indicate a decrease in the surface roughness of the doped Cr_2O_3: Cu thin films. The UV-Vis spectra of the Cu doped-Cr_2O_3 films showed high transparency in the visible region. The optical band gap of Cr_2O_3 thin films decreases with increasing in Cu doping rate. The Nyquist plot shows that the equivalent circuit of Cu doped-Cr_2O_3 films is a parallel circuit R_pC_p. As the concentration of Cu increases, Resistance R_P regresses while capacitance C_p increases.

Keywords: Chromium Oxide, Copper, Sol-gel Dip Coating, thin films

1 Introduction

The world has known a huge technological revolution supported by a great intellectual development, which prompted all officials and researchers to look for the best and search for the most appropriate among the various materials. Among the sciences that have attracted a great deal of interest is the science of materials, especially nanomaterials, which have many uses. Like all metallic oxides, chromium (III) oxide has been the subject of several researches and studies either in nanopowder or in thin layer due to its different and varied characteristics, in particular its thermodynamic stability at high temperatures, chemical resistance, hardness [1], catalytic, medicinal [2] and antiferromagnetic properties with a Curie temperature T_C in the region of 305 to 315 K [3]. In addition, the chromium (III) oxide in the form of thin films can exhibit a p or n-type semiconductor behavior [4]. All these properties make pure or doped chromium dioxide a highly stressed functional material in several fields of applications such as catalyst [5], solar absorber material for the collection of solar energy [6, 7], protective coatings to deal with corrosion and oxidation phenomena [8], air or liquid vibration sensors [9, 10], green pigment [11], an interface tunnel junction barrier [12] and liquid crystal displays [2].

Cr_2O_3 thin films have been prepared by a variety of techniques, among which there can be mentioned microwave irradiation [13], Solvent Free Method [14], precipitation [15, 16], photosynthesis method [17], solution based chemical method [18], Green Synthesis [19], hydrothermal method [20], thermal evaporation [21], solid thermal decomposition [22], electron-beam evaporation [23], flame fusion method [3] and sol - gel method [24]. Recently, the sol–gel process has emerged as one of the best methods for the synthesis of metal oxide materials with particularly important properties [25]. This method allows, according to some studies [26, 27], is a simple, inexpensive and very practical method for the preparation of homogeneous, chemically stable, ultrafine and transparent optical materials. Further modification of the properties of chromium (III) oxide in particular in the form of thin layers by doping with metallic elements has often been solicited by researchers. It has been reported in the literature that doping by copper can contribute to the improvement of some properties, for instance: conductivity [28], photocatalytic activity [29] and optical properties [30].

The novelty of this work is to investigate the effect of Cu incorporation on the structural, morphological, optical and electrical properties of Cr_2O_3 thin films synthesized by sol–gel dip coating technique. The synthe-

***Corresponding Author: Hadj Benhebal:** Département de Chimie, Université Ibn-Khaldoun, Tiaret (14000), Algeria; Email: benhebalh@yahoo.fr
Ahlam Zekaik: Laboratoire de Génie Physique, Université Ibn-Khaldoun, Tiaret (14000), Algeria; Laboratoire Synthèse et Catalyse, Université Ibn-Khaldoun, Tiaret (14000), Algeria
Bedhiaf Benrabah: Laboratoire de Génie Physique, Université Ibn-Khaldoun, Tiaret (14000), Algeria

sized materials were characterized by the following techniques: X-ray powder diffraction (XRD), Infrared spectroscopy (IR), Ultraviolet–visible spectroscopy, impedance spectroscopy.

2 Experimental Methods

2.1 Synthesis

The pure and Cu doped Cr_2O_3 thin films were synthesized and deposited on glass substrate via sol-gel dip coating process using Chromium (III) Nitrate Nonahydrate [$Cr(NO_3)_3{\cdot}9H_2O$] and Copper(II) nitrate trihydrate [$Cu(NO_3)_2{\cdot}3H_2O$] as starting precursor.

The specific preparation process (Figure 1) is:

3,76 g of $Cr(NO_3)_3{\cdot}9H_2O$ and 4,42 g of Sucrose were dissolved in 100 ml deionized water and kept in a continuous state of stirring for 60 min to obtain the Undoped Cr_2O_3 solution.

The solutions of dopant were prepared by dissolving $Cu(NO_3)_2{\cdot}3H_2O$ in 100 ml of deionized water and stirred for 60 min.

Both solutions were mixed with magnetic stirrer for 60 min.

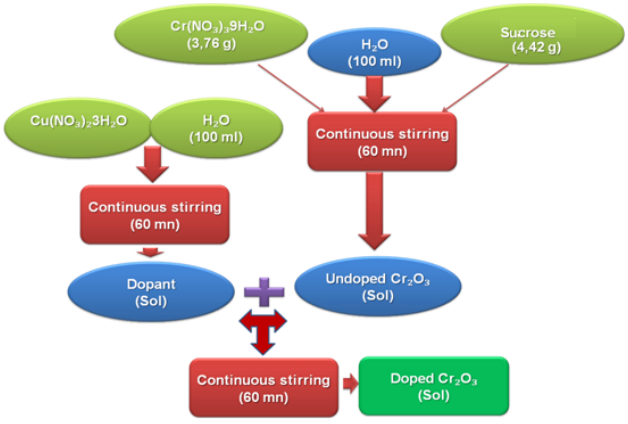

Figure 1: Process for sol–gel synthesis of copper-doped Cr_2O_3.

The second step is to deposit the thin layers on glass substrate. These substrates were well cleaned with acetone, rinsed with distilled water and dried in an oven before being immersed in the solutions. The cleaned glass substrates were immersed vertically in the solution and then removed using the experimental set-up presented in Figure 2. Then, these substrates will be introduced into a furnace whose maximum temperature is fixed at 400°C for eventual calcinations.

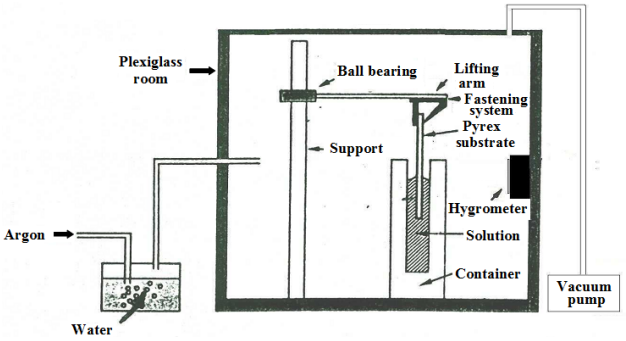

Figure 2: Schematic of the experimental set-up used for the deposition of thin films.

2.1.1 Characterization

As mentioned in the objectives of this work, some characterization techniques have been implemented to highlight the properties of synthesized materials. For XRD analyzes, Rigaku miniflex 600 with Cu-Kα line (λ = 1.5406 Å) was used to determine the nature and the size of crystalline phases of Cr_2O_3. The surface morphology of films has been examined by scanning electron microscopy (SEM) with Joel Jed-2300 and by atomic force microscopy (AFM) using (Nanosurf C300). Absorbance measurements were recorded using a UV-Visible spectrophotometer (Shimadzu 1650). The identification of functional groups of thin films deposited on silicon substrates by infrared spectroscopy was measured using Shimadzu 1800 spectrophotometer. Finally the electrical properties were investigated by impedance measurements realized on an Agilent 4284A LCR-meter.

3 Results and Discussions

a) Structural characterization

The XRD patterns of all the materials of Cr_2O_3 pure and doped by copper at (3%, 6%, 9% and 12%) elaborated by sol-gel dip-coating method are shown in Figure 3. The spectra showed crystalline materials with 2θ peaks lying at 24,42° (012), 33,54° (104), 36,54° (110), 41,46° (113), 50,12° (024), 54,86° (116), 63,62° (214), 65,20° (300). All peaks are identical to those corresponding to the Cr_2O_3 phase indexed in the rhombohedral structure with an R-3c space group, as described in the 072-3533 JCPDS card [31, 32]. The strong intensity of the peaks representing the preferential orientation in the (104), (110) and (116) planes indicates that thin films exhibit good crystallinity [33].

Table 1: Crystallite size of pure and Cu-doped Cr_2O_3.

	Undoped Cr_2O_3	Cr_2O_3:Cu (3%)	Cr_2O_3:Cu (6%)	Cr_2O_3:Cu (9%)	Cr_2O_3:Cu (12%)
Crystallite size (Å)	112	288	269	217	198

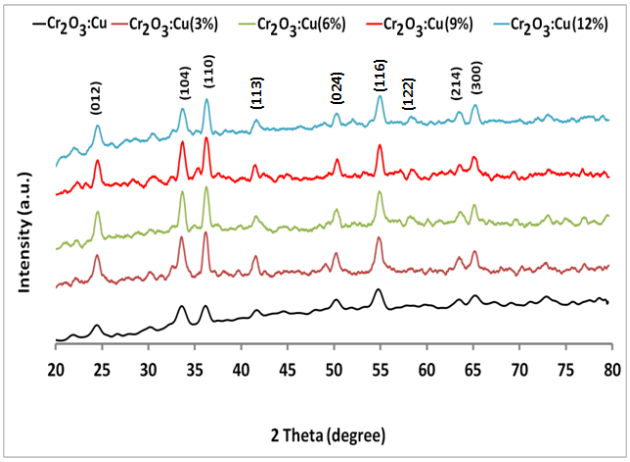

Figure 3: XRD pattern of Undoped and Cu doped Cr_2O_3 thin films.

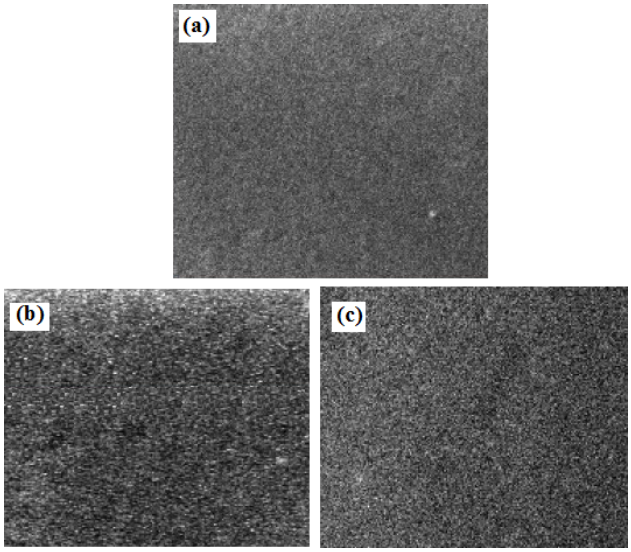

Figure 4: SEM micrographs of Cu-doped Cr_2O_3 films with (a) Cu=0 at.%, (b) Cu=3 at.%, (c) Cu=9 at.%.

Additionally, it is evident that no extra phases corresponding to either copper or copper oxides were detected from this technique. This means that the rhombohedral chromium (III) oxide structure has not been modified by the incorporation of copper and that the Cu^{+2} ions have been substituted in the Cr_2O_3 sites [34].

The average crystallite size, D of the undoped and Cu-doped Cr_2O_3 samples was estimated from the X-ray spectra. D is the average of the values deduced from the three most intense peaks (104), (110) and (116) using the following Scherrer's formula:

$$D = \frac{0,9\lambda}{\beta Cos\theta}$$

where λ is the wavelength of Cu-K radiation (λ = 1.5405 Å), θ the diffraction angle and β the full width of the diffraction line measured at half of its maximum intensity, in radians.

As shown in the Table 1, the crystallite size of the films first, increases and then decreases with increasing in Cu concentration. This result can be justified by the enhanced incorporation of Cu^{2+} ions into the Cr^{3+} sites of the host Cr_2O_3 lattice [35]. This decrease in grain size with the increase in Cu concentration reflects degradation in the crystalline quality of the thin layers and consequently the increase in grain boundary scattering [36].

The surface morphology of three samples (undoped and doped at 3 and 9%) were analyzed by using SEM. From images shown in Figure 4, it was found that the undoped Cr_2O_3 film had a surface more or less smooth. For the others, it is clear that the surface morphology of the films strongly depends on the Cu content [37], as long as these films seem to have more porosity compared to the undoped film.

Three-dimensional (3D) AFM images of Cu doped chromium oxide thin films are presented in Figure 5. From the AFM measurements, it appears that the surface morphology predicts compact nanocrystalline structure [38]. It should also be noted that by the increasing of Cu doping concentration (Figure 6), the surface roughness is decreased, which is attributed to the decrease of grain size [39].

b) Optical properties

The optical transmittance spectra (Figure 7) were recorded in the 290 - 900 nm spectral range for sol-gel undoped and cu-doped Cr_2O_3 thin films grown on glass substrates with different Cu doping concentrations (0, 3, 6, 9 and 12 at%). The films prepared with a doping rate of 0, 3 and 6% show good optical transmittance with a transparency around 98%. This transmittance begins to decrease progressively as the concentration of copper increases and a minimum value of 90% is obtained for the film coated with 12 at%

Table 2: Band gap energy of undoped and doped Cr_2O_3 thin films.

	Undoped Cr_2O_3	Cr_2O_3:Cu (3%)	Cr_2O_3:Cu (6%)	Cr_2O_3:Cu (9%)	Cr_2O_3 :Cu (12%)
Eg (eV)	2,94	2,92	2,89	2,73	2,51

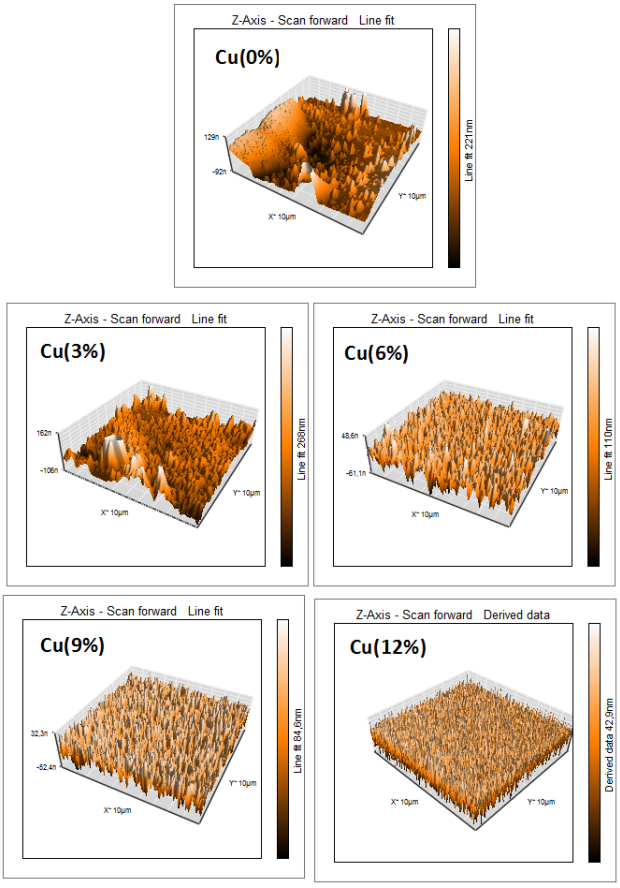

Figure 5: Three-dimensional AFM images of Cr_2O_3 thin films with various Cu doping concentrations.

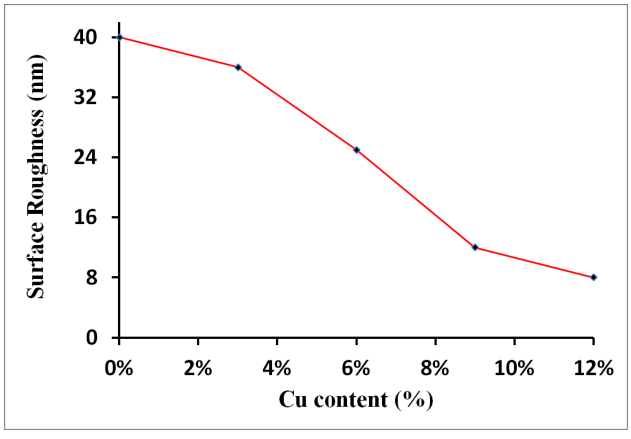

Figure 6: Plot of RMS roughness *vs*. Cu content.

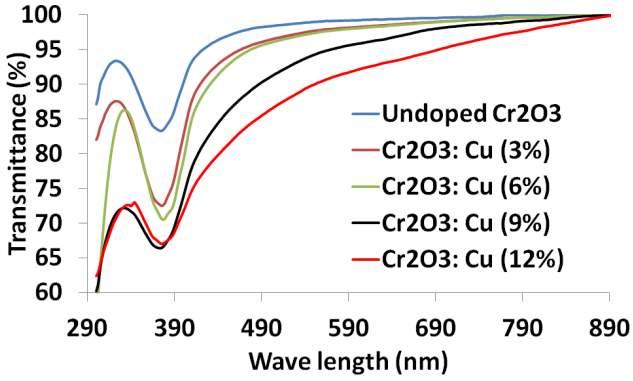

Figure 7: Transmittance spectra of Undoped and Cu doped Cr_2O_3 thin films.

Cu. This decrease in the transmittance can be related to the increased scattering of photons by crystal defects by doping [40].

In optical devices, band gap energy remains one of the main characteristics of the synthesized materials, which must be determined [41]. The optical band gap energy of the materials was determined by means of the Tauc's equation, which translates the relation between the absorption coefficient (α) and the incident energy ($h\nu$). This relation is given by the equation [42]:

$$(\alpha h\nu)^2 = B(h\nu - Eg),$$

where B is constant and has different values for different transitions, $h\nu$ is the photon energy and Eg is the optical band gap energy. The variation of $(\alpha h\nu)^2$ with photon energy ($h\nu$) for all synthesized films is shown in Figure 8 and the results are grouped in Table 2.

From the results appearing on the Table 2, the value of the optical band gap energy (Eg) of the undoped sample is found to be equal to 2,94 eV. This value is very close to those cited by several authors [43]. For the doped thin films, optical energy band gap goes on decreasing with increasing Cu content. This decrease can be related to the average bond energy which is itself a function of the composition and consequently to the doping content [44, 45].

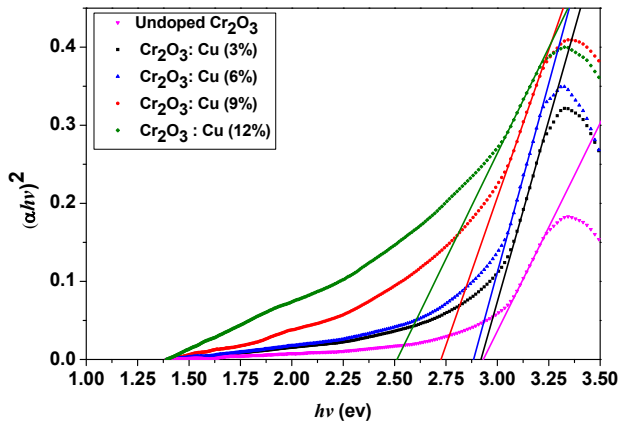

Figure 8: Direct band gap of the Undoped and Cu doped Cr_2O_3 thin films.

c) Infrared Spectrum Analysis

Figure 9 shows the FT-IR spectra of pure and copper doped chromium (III) oxide thin films calcined at 400°C. It seems clear that the spectra of all samples have the position of the peaks at the same wavenumber confirming no change in the structural bonding upon doping [46]. The absorption bands at wave numbers smaller than 800 cm^{-1} are related to M-O bands [47], which are the result from the Cr-O stretching modes, which confirms the formation of crystalline chromium (III) oxide [48]. This result is consistent with those obtained by other researchers [49], who estimate that metal oxide Cr_2O_3 generally reveal absorption bands below 1000 cm^{-1} due to inter-atomic vibrations. The peak that appears around 2350 cm^{-1} is due to νO=C=O present in the air adsorbed during preparation [13].

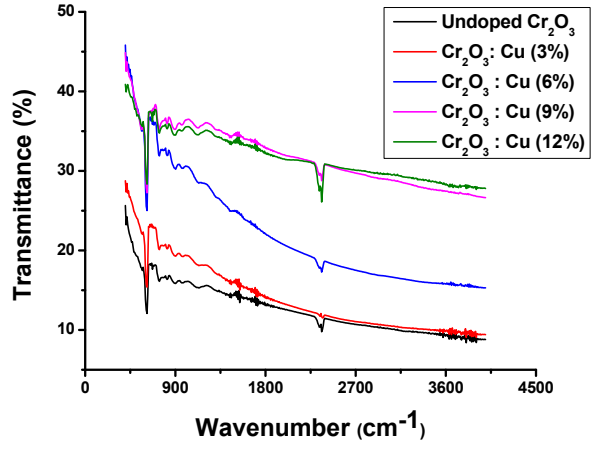

Figure 9: Infrared Spectrum of undoped and doped Cr_2O_3 thin films.

d) Impedance spectra

Figure 10 is the Nyquist representation of the undoped Cr_2O_3 thin films and doped with copper whose frequency varies from 75 KHz to 30 MHz at ambient temperature (20°C). The various processes taking place at the electrode / electrolyte interface can be modeled by the construction of an equivalent electrical circuit. The physical logic of the system indicates that concurrent processes are connected in parallel. This figure is characteristic of a parallel RC circuit, where C_p is the capacitance and R_p is its resistance. Two conduction mechanisms are present at the same time, conduction through grains and conduction through grain boundaries [50]. In addition, the size of the grains is reduced under the effect of doping, which introduces more joints in the samples, which will make the effect of the grain boundaries in the samples more dominant than the contribution of the grains [51].

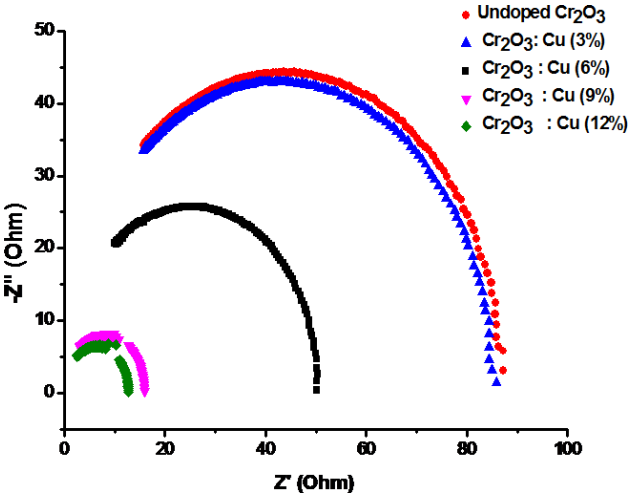

Figure 10: Nyquist plots of of undoped and doped Cr_2O_3 thin films.

The capacity of chromium oxide films in the different samples was determined by means of the following equation:

$$C_p = \frac{1}{2\pi f_{max} R_P}, \quad \text{where } f_{max} \text{ is the maximum frequency.}$$

The graphical illustration (Figure 11) of the results grouped in Table 3 shows that the resistance R_P decreases with the increase in the doping rate and reaches the value of 12.8 Ω for a doping rate of 12%, while the capacity C_P increases to a value of 24.2 nF for the same doping rate. The variation in capacity can be ascribed to the formation of oxygen vacancies caused by the substitution of Cr^{3+} by Cu^{2+} ions at the surface of the grains [52].

Table 3: Variation of resistance and capacity of undoped and doped Cr_2O_3 thin films.

	f (KHz)	R (Ω)	C (nF)
Undoped Cr_2O_3	485	87	3.77
Cu-doped Cr_2O_3 (3%)	490	85.5	3.79
Cu-doped Cr_2O_3 (6%)	515	50.2	6.15
Cu-doped Cr_2O_3 (9%)	505	16	19.7
Cu-doped Cr_2O_3 (12%)	515	12.8	24.2

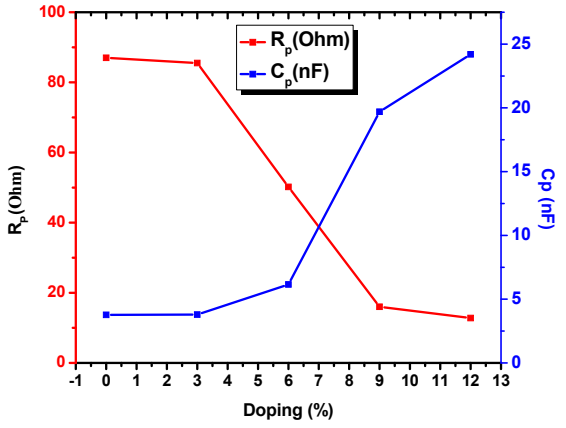

Figure 11: Variation of resistance and capacity of undoped and doped Cr_2O_3 thin films.

4 Conclusions

Cu: Cr_2O_3 thin films are successfully deposited on glass substrates by sol-gel dip coating method starting from Chromium (III) Nitrate Nonahydrate and Copper (II) nitrate trihydrate. The effect of copper doping on structural, optical and electrical properties has been studied. The results of X-ray diffraction study show that the rhombohedral structure of the crystal structure of Cr_2O_3 is preserved; on the other hand, the average crystallite size has undergone some changes. The deposits were uniform with a more or less smooth surface morphology. The surface roughness, as quantified by atomic force microscopy (AFM), was found to decrease with increasing Cu content. Doping Cr_2O_3 thin films with Cu resulted in an improvement of their transparency in the visible range and a reduction of optical band gap energy, which shift from 2.94 to 2.51 eV. IR spectra revealed the formation of Cr_2O_3 by the appearance of the peak related to the Cr-O stretching modes. Finally, the results of impedance spectroscopy study show that the dissolution of the copper ions in the chromium oxide lattice has created oxygen point defects which control the degree of densification of the films.

References

[1] G. Carta, M. Natali, G. Rossetto, P. Zanella, G. Salmaso, S. Restello, et al., Chem. Vapor. Dep., 11 (2005) 375-380.
[2] T. M. Al-Saadi, Adv. Phys. Theor. Appl., 44 (2015) 139-148.
[3] T. R. Mcguire, E. J. Scott, and F. H. Grannis, Phys. Rev., 102 (1956) 1000-1003.
[4] P. Kofstad and K. P. Lillerud, J. Electrochem. Soc. 127(1980) 2410-2419.
[5] M. R. Kantserova, N. V. Grabovaya, S. V. Kolotilov, and S. N. Orlik, Theor. Exper. Chem., 45 (2009) 368-372.
[6] R. Koksbang and P. Norby, Electrochem. Acta, 36 (1991) 127-133.
[7] V. Teixeira, E. Sousa, M. Costa, F. C. Nunes, L. Rosa, M. J. Carvalho, et al., Thin. Solid. Films., 392 (2001) 320-326.
[8] F. D. Lai, C. Y. Huang, C. M. Chang, L. A. Wang, and W. C. Cheng, Microelecton. Eng., 17 (2003) 67-68.
[9] V. A. Karpina, V. I. Lazorenko, C. V. Lashkarev, V. D. Dobrowolski, L. I. Kopylova, V. A. Baturin, et al., Cryst. Res. Technol., 39 (2004) 980-992.
[10] A. Gupta, B.C. Kim, E. Edwards, C. Brantley, and P. Rufln, Mat. Sci. Eng. B., 177 (2012) 1583-1588.
[11] I. F. Jeffry, L. Ning, and D. Daniel, Biochem., 38 (1999) 11593-11596.
[12] T. Yu, X Z. Shen, J. He, W. X. Sun, S. H. Tang, and J. Y. Lin, J. App. Phys, 93 (2003) 3951- 3953.
[13] J. T. Anandhi, S. L. Rayer, and T. Chithambarathanu, Chem. Mat. Eng., 5 (2017) 43-54.
[14] R. Meenambika, S. Ramalingom, and Chithambara Thanu, Int. J. Eng. Res. Appl., 4 (2014) 20-23.
[15] R. Chaplin, P. R. Chapman, and R. H. Griflth, Math. Phys. Eng. Sci., 224 (1954) 412-419.
[16] V. S. Jaswal, A. K. Arora, M. Kinger, V. D. Gupta and J. Singh, Oriental. J. Chem, 30 (2014) 559-566.
[17] H. I. Abdellah and L. J. Abbas, Int. J. Appl. Phys. Bio-Chem. Res, 7 (2017) 1-8.
[18] M. A. Raza, Z. Kanwal, S. Riaz, and S. Naseem, ACEM, (2016).
[19] C. Ramesh, K. Mohan Kumar, N. Latha, and V. Ragunathanand, Current. Nanoscience, 8 (2012) 603-607.
[20] M. M. Abdullah, M. Fahd Rajab, and M. Saleh Al-Abbas, AIP Adv., 4 (2014) 027121.
[21] M. Julkarnain, J. Hossain, K. S. Sharif, and K. A. Khan, Canadian., J. Chem. Eng. Techn., 3 (2012) 81-85.
[22] L. Li, Z F. Yan, Q. Gao Lu, and H. Zhong Zhu, J. Phys. Chem. B., 110 (2006) 178-183.
[23] M. F. Al-Kuhaili and S. M. A. Durrani, Optical. Mat., 29 (2007) 709-713.
[24] F. Ravish and A. Riaz, Glob. J. Zool., 2 (2017) 8-12.
[25] I. John Berlin and K. Joy, Phys. B., 457 (2015) 182-187.
[26] R. Ashiri, A. Nemati, M. Sasani Ghamsari, and M. M. Dastgahi, J Mater Sci: Mater Electron, 25 (2014) 5345-5355.
[27] R. Ashiri, Metall and Mat Trans A, 43 (2012) 4414-4426.
[28] S. J. Wen, G. Couturier, G. Campet, J. Portier, and J. Claverie, Phys. Stat. Sol., 130 (1992) 407-414.
[29] Y. Wang, W. Duan, B. Liu, X. Chen, F. Yang, and J. Guo, J. Nanomaterials., 2014 (2014) 178152.
[30] P. Maddahi, N. Shahtahmasebi, A. Kompany, M. Machreghi, S. Safaee, and F. Roozban, Mat. Sci. Poland., 32 (2014) 130-135.
[31] P. Gibot and L. Vidal, J. Eur. Ceramic. Soc., 30 (2010) 911-915.

[32] J. Mollicone, F. Ansart, P. Lenormand, B. Duployer, C. Tenailleau, and J. Vicente, J. Eur. Ceramic. Soc., 34 (2014) 3479–3487.
[33] H. Gómez-Pozos, E. J. Luna Arredondo, A. M. Álvarez, R. Biswal, Y. Kudriavtsev, J. V. Pérez, et al., Materials, 9 (2016) 1-16.
[34] T. Saidani, M .Zaabat, M. S. Aida and B. Boudine, Superlattices. Microstruct., 88 (2015) 315-322.
[35] K. Kavitha, T. Subba Rao, and R. Padmasuvarna, J. Nanosci. Nanotechno. App, 1 (2017) 1-3.
[36] N. Manjula, M. Pugalenthi, V. S. Nagarethinam, K. Usharani, A. R. Balu, Mat. Sci. Poland, 33 (2015) 774-781.
[37] R. K. Shukla, A. Srivastava, N. Kumar, A. Pandey, and M. Pandey, J. Nanotechnology., 2015 (2016) 1- 10.
[38] R. Ashiri, Metall and Mat Trans A, 45 (2014) 4138-4154.
[39] T. Saidani, M. Zaabat, M.S. Aida b, B. Boudine, Superlattices and Microstructures, 88 (2015) 315-322.
[40] S. Jeetendra, H. Nagabhushana, K. Mrudula, C. S. Naveen, P. Raghu, and H. M. Mahesh, Int. J. Electrochem. Sci., 9 (2014) 2944-2954.
[41] R. Ashiri, A. Nemati, M. Sasani Ghamsari, and H. Aadelkhani, Journal of Non-Crystalline Solids, 355 (2009) 2480–2484.
[42] J. Tauc, Amorphous and Liquid Semiconductors, New York: Plenum, (1974).
[43] C. Huaqiang, Q. Xianqing, L. Yu, Z. Meijuan, and Z. Qiming, Applied. Phys. Letters., 88 (2006) 241112.
[44] M. M. Hafiz, N. El-kabany, H. Mahfoz.Kotb, and Y. M. Bakier, Int. J. Thin. Fil. Sci. Tec., 4 (2015) 179-185.
[45] A. K. Pattanaik and A. Srinivasan, J. Optoelectron, Adv. Mater. 5 (2003) 1161-1167.
[46] K. Kumar, N. Kumar Singh, H. S. Park, and O. Parkash, RSC Adv., 55 (2016) 1-8.
[47] R. Ashiri, Vibrational Spectroscopy, 66 (2013) 24-29.
[48] M. A. Henderson, Surf. Sci., 604 (2010) 1800-1807.
[49] F. Farzaneh and M. Najafi, J. Sci, Islamic. Republic. Iran, 22 (2011) 329-333.
[50] L. Beaunier, I. Epelboin, J. C. Lestrade, and H. Takenouti, Surf. Tech., 4 (1976) 237-254.
[51] B. Benrabah, A. Bouaza, A. Kadari, and M. A. Maaref, Superlattices. Microstruct., 50 (2011) 591-600.
[52] R. Muccillo, J. A. Cerri, E. R. Leite, E. Longo, and J. A. Varela, Mat. Letters, 30 (1997) 125-130.